

Application of Adaptive Beamforming Techniques to HF Radar

Peter Vouras and Brian Freburger
Naval Research Laboratory, Radar Division
Washington D.C., 20375, USA

phone: +(202)404-1859, email: peter.vouras@nrl.navy.mil, brian.freburger@nrl.navy.mil

Abstract—This paper evaluates the performance of several adaptive beamforming techniques applied to the problem of cancelling interference in a High Frequency (HF) radar with transmitter and receiver physically separated by large distances. The difficulties posed by mitigating interference in a HF radar are fundamentally different in many aspects from the adaptive cancellation problem in more conventional phased array radars operating at higher frequencies. Some of the issues specific to adaptive cancellation in HF radar will be addressed in this paper and performance results will be presented using measured data.

Index Terms— adaptive beamforming, HF radar, self-interference.

I. INTRODUCTION

The basic operating principle of HF radar is the reflection of transmitted electromagnetic radiation off the ionospheric layer of the atmosphere onto a target located hundreds or thousands of miles away. Energy scattered by the target is reflected back along the same path and can be collected by a receiver collocated with the transmitter, or it can be detected by a receiver placed closer to the target as depicted in Fig. 1. The bistatic radar configuration shown in Fig. 1 is similar to the HF radar systems previously described in [1] and [2]. This particular HF radar configuration will be denoted as Forward Based Bistatic (FBB-) HF Radar in this paper.

Advantages of the FBB-HF radar configuration are that the receiver can be assembled quickly using just a few array elements and its proximity to the target provides opportunities for enhanced signal gain. However, a unique problem associated with the FBB-HF radar is that there exists a direct path from the transmitter to the receiver via the ionosphere that results in the receiver detecting a strong coherent signal that may mask the intended target. The purpose of this paper is to investigate and evaluate 11 adaptive processing algorithms which may be used to cancel the direct signal interference. An additional complicating factor is that the directions of the direct signal interference and the target are unknown to the radar and must be estimated such that a null is placed in the array pattern in the correct direction and the main beam gain is placed on the target. Furthermore, the ionosphere is a highly nonstationary random medium that will

introduce errors in the presumed angles of arrival (AOAs) of the target signal and interference. These errors may seriously degrade canceller performance. Therefore, any adaptive processing scheme must be robust to the presence of these errors, as well as the typical random errors always present in the array manifold. A practical adaptive processing scheme must also be robust to a potential mismatch between the adaptive weights, computed using a finite number of data samples, and the actual data samples to which the weights are applied, which are usually different and separated in time.

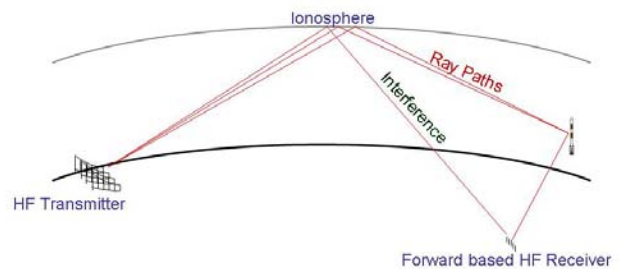


Figure 1 – FBB-HF Radar

As mentioned previously, the adaptive processing schemes evaluated for this paper were compared using measured data. This data was collected from an HF array with 6 elements operated by the Naval Research Lab in a FBB-HF configuration. The radar transmits a continuous train of Linear FM (LFM) chirps. Stretch processing is performed in the receiver by mixing with a deramping signal $s(k)$, and then the computed adaptive weights, $w_i(k)$, are applied independently to each array element as shown in Fig. 2. Subsequently, a FFT is performed along the range dimension and then the adapted array element output is summed in a conventional beamformer.

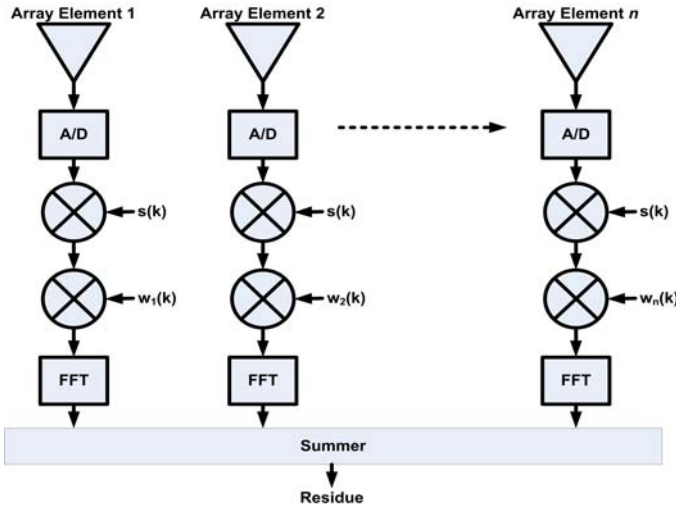


Figure 2 – Time Domain Post-Stretch Beamforming Architecture

The computed adaptive weights may be applied recursively or using batch updates. Batch update procedures accumulate a blocked version of the input data to train the adaptive weights and then apply the computed weights retroactively to the data. The advantage of batch update algorithms is that they result in a higher Signal-to-Interference-plus-Noise (SINR) at the output of the beamformer. Recursive algorithms update and apply the adaptive weights at every time sample. The advantage of recursive algorithms is that they are computationally less expensive and easier to implement.

A total of eleven adaptive beamforming algorithms were evaluated for this paper. These include batch updating algorithms such as Covariance Matrix Taper (CMT), Eigenvalue Thresholding, Diagonal Loading, Time Domain Segmenting, Frequency Domain beamforming, Minimum Variance Distortionless Response (MVDR), and the Lorenz beamformer. Recursive algorithms considered include conventional Recursive Least Squares (RLS), RLS with Variable Loading (RLS-VL), conventional Least Mean Square (LMS), and LMS with Scaled Projection (LMS-SP).

Fig. 3 is a scroll plot illustrating some typical target tracks collected from the FBB-HF radar without any adaptive cancellation applied. This figure shows the output in 7 range bins for a duration of 90 seconds. Along the horizontal axis is plotted the Doppler frequency in each range bin from -20 Hz to +20 Hz. The strong direct signal interference is visible at 0 Hz Doppler in each range bin. The target track is visible in range bins 5 and 6.

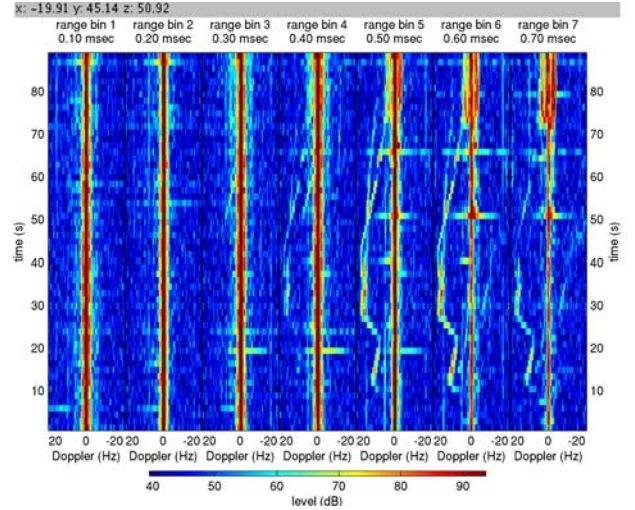


Figure 3 – Unadapted Array Output

II. BRIEF SUMMARY OF ALGORITHMS

In this section a brief description of the algorithms evaluated will be provided.

A. Minimum Variance Distortionless Response

The MVDR beamformer minimizes the mean square value of the array output while constraining the beam to produce a distortionless response in the desired look direction. The Sample Matrix Inversion (SMI) solution is obtained by [3],

$$\mathbf{w} = \frac{\hat{\mathbf{R}}^{-1} \mathbf{s}}{\mathbf{s}^H \hat{\mathbf{R}} \mathbf{s}}$$

where $\hat{\mathbf{R}}$ is the maximum likelihood estimate of the data covariance matrix and \mathbf{s} is the target steering vector. Specifically,

$$\hat{\mathbf{R}} = \frac{1}{N} \sum_{j=1}^N \mathbf{x}_j \mathbf{x}_j^H$$

where \mathbf{x}_j denotes a vector of spatial samples across the array elements at one time instant.

B. Least Mean Square Beamformer

The weights in the LMS algorithm are updated after each sampling interval by adding a small increment to the old weights. The increment is proportional to the rate of change of the output residue power with respect to the weight being updated. LMS adaptation has low computational complexity but can be slow to converge.

The following paragraphs will summarize the more detailed development of LMS beamformers which can be found in [3] or [4]. Let \mathbf{x}_k denote the N -by-1 vector of signals received by an array of N sensors. The beamformer output obtained after applying a complex weight to the output of each array element and summing across all the elements is, $y_k = \mathbf{w}^H \mathbf{x}_k$. In this case, the weights w_i are chosen to minimize the array output power subject to a set of m linear constraints of the form $\mathbf{C}^H \mathbf{w} = \mathbf{f}$, where \mathbf{C} is the N -by- m constraint matrix and \mathbf{f} is the m -by-

1 vector of constraint values. For the LMS algorithm results described later in this paper, $\mathbf{f} = [1 \ 0]^T$.

The optimization problem to be solved can be written as

$$\mathbf{w} = \arg \min \mathbf{w}^H \mathbf{R} \mathbf{w}$$

$$\text{s.t. } \mathbf{C}^H \mathbf{w} = \mathbf{f}$$

where $\mathbf{R} = E\{\mathbf{x}_k \mathbf{x}_k^H\}$ is the data covariance matrix. The optimal solution is

$$\mathbf{w} = \mathbf{R}^{-1} \mathbf{C} (\mathbf{C}^H \mathbf{R}^{-1} \mathbf{C})^{-1} \mathbf{f}.$$

The weight vector \mathbf{w} can be decomposed into two components; one within the constraint subspace, \mathbf{w}_q , and one orthogonal to it, \mathbf{w}_a . In other words, $\mathbf{w} = \mathbf{w}_q - \mathbf{B} \mathbf{w}_a$. The columns of the N -by- $(N-m)$ matrix \mathbf{B} form a basis for the orthogonal complement of the range space of \mathbf{C} , implying that $\mathbf{B}^H \mathbf{C} = \mathbf{0}$. The $(N-m)$ -by-1 vector \mathbf{w}_a can adapt freely to improve interference suppression in the $(N-m)$ -dimensional orthogonal subspace. The vector \mathbf{w}_q is fixed and equal to,

$$\mathbf{w}_q = \mathbf{C} (\mathbf{C}^H \mathbf{C})^{-1} \mathbf{f}.$$

Now, the original constrained optimization problem can be reformulated as the unconstrained problem,

$$\mathbf{w}_a = \arg \min (\mathbf{w}_q - \mathbf{B} \mathbf{w}_a)^H \mathbf{R} (\mathbf{w}_q - \mathbf{B} \mathbf{w}_a)$$

with optimal solution given by

$$\mathbf{w}_a = (\mathbf{B}^H \mathbf{R} \mathbf{B})^{-1} \mathbf{B}^H \mathbf{R} \mathbf{w}_q.$$

Computationally, at each iteration k the LMS algorithm proceeds as follows [4],

1. $\mathbf{w}_a(0) = \mathbf{0}$.
2. $y_c(k) = \mathbf{w}_q^H \mathbf{x}(k)$
3. $\mathbf{z}(k) = \mathbf{B}^H \mathbf{x}(k)$
4. $y_p(k) = y_c(k) - \mathbf{w}_a^H(k-1) \mathbf{z}(k)$
5. $\mathbf{w}_a(k) = \mathbf{w}_a(k-1) + \alpha z(k) y_p^*(k)$, where α is a judiciously chosen step size, e.g. $\alpha = 1 / (N \|\mathbf{x}\|^2)$.
6. $\mathbf{w}(k) = \mathbf{w}_q - \mathbf{B} \mathbf{w}_a(k)$.

C. LMS Scaled Projection Algorithm

The LMS-SP algorithm improves robustness to pointing errors and to random perturbations in array parameters by enforcing an upper bound on the norm of the weight vector. This constraint is imposed on the adaptive portion of the weight vector by reducing its length and maintaining its direction.

Computationally, the LMS-SP algorithm proceeds as follows [4],

1. $\mathbf{w}_a(0) = \mathbf{0}$.
2. $y_c(k) = \mathbf{w}_q^H \mathbf{x}(k)$
3. $\mathbf{z}(k) = \mathbf{B}^H \mathbf{x}(k)$
4. $y_p(k) = y_c(k) - \mathbf{w}_a^H(k-1) \mathbf{z}(k)$
5. $\mathbf{w}_a(k) = \mathbf{w}_a(k-1) + \alpha z(k) y_p^*(k)$, where α is a judiciously chosen step size, e.g. $\alpha = 1 / (N \|\mathbf{x}\|^2)$.
6. If $\|\tilde{\mathbf{w}}_a(k)\|^2 \leq \beta^2$, then $\mathbf{w}_a(k) = \tilde{\mathbf{w}}_a(k)$. Else if, $\|\tilde{\mathbf{w}}_a(k)\|^2 > \beta^2$, then $\mathbf{w}_a(k) = \tilde{\mathbf{w}}_a(k) \cdot (\beta / \|\tilde{\mathbf{w}}_a(k)\|)$. Here β is the upper bound constraint on the norm-squared of \mathbf{w}_a .
7. $\mathbf{w}(k) = \mathbf{w}_q - \mathbf{B} \mathbf{w}_a(k)$.

Figure 4 illustrates the evolution of the norm squared of \mathbf{w}_a as the algorithm is applied to the HF radar data evaluated for this paper.

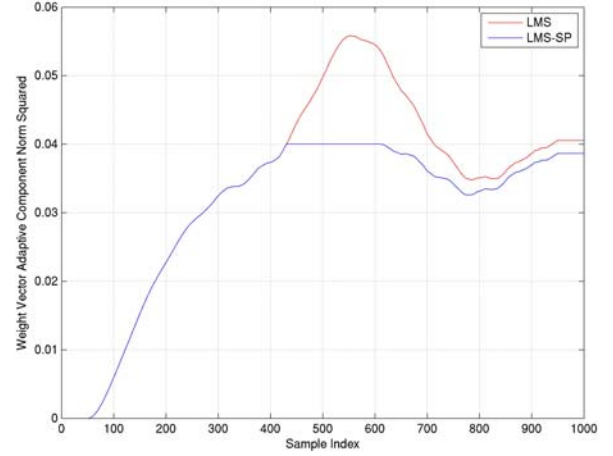


Figure 4 – Evolution of LMS-SP Adaptive Weight Vector

D. Recursive Least Squares Beamformer

The RLS beamformer iteratively updates an estimate, \mathbf{P} , of the inverse of the data covariance matrix without explicitly computing a matrix inverse. RLS adaptation is quicker to converge than LMS but is more computationally complex. The RLS beamformer is more sensitive to mismatch between the array response and the constraints used to place desired nulls than the LMS algorithm.

Numerically, the RLS algorithm proceeds as follows [4],

1. $\mathbf{w}_a(0) = \mathbf{0}$, $\mathbf{P}(0) = \mathbf{I}_{N-m}$.
2. $y_c(k) = \mathbf{w}_q^H \mathbf{x}(k)$
3. $\mathbf{z}(k) = \mathbf{B}^H \mathbf{x}(k)$
4. $y_p(k) = y_c(k) - \mathbf{w}_a^H(k-1) \mathbf{z}(k)$
5. $\mathbf{g}(k) = \mathbf{P}(k-1) \mathbf{z}(k) / (\mu + \mathbf{z}^H(k) \mathbf{P}(k-1) \mathbf{z}(k))$ where μ was set equal to 1.
6. $\mathbf{P}(k) = \mu^{-1} (\mathbf{P}(k-1) - \mathbf{g}(k) \mathbf{z}^H(k) \mathbf{P}(k-1))$
7. $\mathbf{w}_a(k) = \mathbf{w}_a(k-1) + \mathbf{g}(k) y_p^*(k)$
8. $\mathbf{w}(k) = \mathbf{w}_q - \mathbf{B} \mathbf{w}_a(k)$.

E. RLS Variable Loading Algorithm

The RLS-VL beamformer is similar to the LMS-SP in that it enforces an upper bound on the norm of the weight vector. If the length of the adaptive portion of the weight vector exceeds its limit, the RLS-VL algorithm scales it back but also seeks the direction within the constraint space that minimizes the value of the objective function. Conceptually, Fig. 5 illustrates the difference between the LMS-SP and the RLS-VL algorithm.

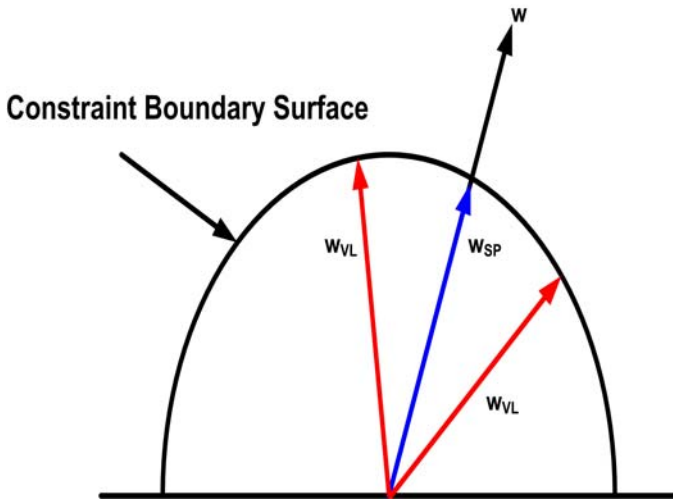


Figure 5 – RLS-VL Weight Vector

Computationally, the RLS-VL algorithm proceeds as follows [4],

1. $\mathbf{w}_a(0) = \mathbf{0}$, $\mathbf{P}(0) = \mathbf{I}_{N-m}$.
2. $y_c(k) = \mathbf{w}_q^H \mathbf{x}(k)$
3. $\mathbf{z}(k) = \mathbf{B}^H \mathbf{x}(k)$
4. $y_p(k) = y_c(k) - \mathbf{w}_a^H(k-1)\mathbf{z}(k)$
5. $\mathbf{g}(k) = \mathbf{P}(k-1)\mathbf{z}(k) / (\mu + \mathbf{z}^H(k)\mathbf{P}(k-1)\mathbf{z}(k))$ where μ was set equal to 1.
6. $\mathbf{P}(k) = \mu^{-1}(\mathbf{P}(k-1) - \mathbf{g}(k)\mathbf{z}^H(k)\mathbf{P}(k-1))$
7. $\tilde{\mathbf{w}}_a(k) = \mathbf{w}_a(k-1) + \mathbf{g}(k)y_p^*(k)$
8. If $\|\tilde{\mathbf{w}}_a(k)\|^2 \leq \beta^2$, then $\mathbf{w}_a(k) = \tilde{\mathbf{w}}_a(k)$. Else,

$$\mathbf{v}(k) = \mathbf{P}(k)\tilde{\mathbf{w}}_a(k),$$

$$a = \|\mathbf{v}(k)\|^2$$

$$b = -2 \cdot \text{Real}\{\mathbf{v}(k)^H \tilde{\mathbf{w}}_a(k)\}$$

$$c = \|\tilde{\mathbf{w}}_a(k)\|^2 - \beta^2$$

$$\lambda(k) = (-b - \text{Real}\{\sqrt{b^2 - 4ac}\}) / (2a)$$

$$\mathbf{w}_a(k) = \tilde{\mathbf{w}}_a(k) - \lambda(k)\mathbf{v}(k)$$
9. $\mathbf{w}(k) = \mathbf{w}_q - \mathbf{B}\mathbf{w}_a(k)$.

F. Diagonal Loading

In this beamformer, the sample covariance matrix is replaced by the diagonally loaded matrix [5]

$$\hat{\mathbf{R}}_{DL} = \hat{\mathbf{R}} + \epsilon \mathbf{I}$$

where $\epsilon > 0$ is the loading factor. Diagonal loading introduces substantial robustness to small sample support and avoids the degradation in antenna sidelobe levels seen with direct application of the SMI algorithm. This degradation is caused by errors in the estimates of the noise subspace eigenvalues. Unfortunately, diagonal loading is not robust to deviations in the estimated interference pointing angle. It is also difficult to choose the loading factor well.

G. Mailloux-Zatman Covariance Matrix Taper

For this algorithm, the original sample covariance matrix is modified as follows [6],

$$\hat{\mathbf{R}}_{MZ} = \hat{\mathbf{R}} \circ \mathbf{T}_{MZ}$$

where \circ denotes the Haddamard product and

$$[\mathbf{T}_{MZ}]_{mn} = \frac{\sin((m-n)\Delta)}{(m-n)\Delta}, \quad \Delta > 0.$$

The CMT algorithm widens the width of the adaptive null. This approach is useful when a mismatch exists between the sample support used for training the beamformer and the data to which the weights are applied.

H. Eigenvalue Thresholding

To summarize the computational steps of this algorithm, first, modify the estimated covariance matrix \mathbf{R} as,

$$\mathbf{R} = \mathbf{D}\mathbf{V}\mathbf{V}^H$$

using an eigendecomposition where $\mathbf{D} = \text{diag}(\lambda_1, \lambda_2, \dots, \lambda_n)$ is the diagonal matrix of eigenvalues with $\lambda_1 \geq \lambda_2 \geq \dots \geq \lambda_n$. Next let,

$$\mathbf{D}_{THR} = \text{diag}(\lambda_1, \max(\mu\lambda_1, \lambda_2), \dots, \max(\mu\lambda_1, \lambda_n))$$

where μ equals the inverse of the condition number of \mathbf{R} .

Now construct a modified covariance matrix, \mathbf{R}_{THR} , as

$$\mathbf{R}_{THR} = \mathbf{V}\mathbf{D}_{THR}\mathbf{V}^H.$$

The performance of this beamformer is similar to that with diagonal loading.

I. Time Domain Segmenting

Divide all the Analog-to-Digital Converter (ADC) samples into multiple nonoverlapping fixed windows [7]. The windows correspond to frequency subbands and this algorithm is analogous to conventional band partitioned beamforming. The computed weights are applied retroactively to all the samples in a block.

J. Lorenz Beamformer

This beamformer explicitly models uncertainty in the array manifold via an ellipsoid. The algorithm can be expressed as a second-order cone program and minimizes the array output power subject to the constraint that the main beam gain exceeds a lower bound for all array responses within the ellipsoid. Mathematically, its statement is

$$\text{minimize } \mathbf{w}^H \mathbf{R} \mathbf{w}$$

$$\text{s.t. } \text{Re}\{\mathbf{w}^H \mathbf{a}(\theta)\} \geq 1 \text{ for all } \mathbf{a}(\theta) \in \Omega.$$

Here, Ω represents the ellipsoid that covers the possible range of values for $\mathbf{a}(\theta)$. The vector $\mathbf{a}(\theta)$ represents the response of the array to a plane wave of unit amplitude arriving from direction θ and is referred to as the array manifold.

Summarizing the relevant development in [8], for a uniform linear array with 6 elements centered at the origin, $\mathbf{a}(\theta)$ can be written as,

$$\mathbf{a}(\theta) = \left[e^{-j\frac{5\varphi}{2}}, e^{-j\frac{3\varphi}{2}}, \dots, e^{j\frac{3\varphi}{2}}, e^{j\frac{5\varphi}{2}} \right]^T$$

where $\varphi = \pi \sin \theta$. The ellipsoid in \mathbf{R}^n containing the array response can be parameterized in terms of a center \mathbf{c} in \mathbf{R}^n and a symmetric non-negative definite configuration matrix \mathbf{P} in $\mathbf{R}^{n \times n}$ as

$$\mathbf{E}(\mathbf{c}, \mathbf{P}) = \left\{ \mathbf{P}^{\frac{1}{2}} \mathbf{u} + \mathbf{c}; \|\mathbf{u}\| \leq 1 \right\}.$$

For $N = 100$ equally spaced samples of the array response at angles between $\theta_{\min} = -5^\circ$ and $\theta_{\max} = 5^\circ$, then

$$\mathbf{c} = \frac{1}{N} \sum_{i=1}^N \mathbf{a}(\theta_i)$$

$$\mathbf{P} = \frac{1}{\alpha N} \sum_{i=1}^N (\mathbf{a}(\theta_i) - \mathbf{c})(\mathbf{a}(\theta_i) - \mathbf{c})^H$$

with $\alpha = 1$ and

$$\theta_i = \theta_{\text{nom}} + \left(-\frac{1}{2} + \frac{i-1}{N-1}\right)(\theta_{\max} - \theta_{\min}),$$

$$1 \leq i \leq N$$

where $\theta_{\text{nom}} = 0^\circ$.

For purposes of computation, the weight vector \mathbf{w} and the values of the array manifold $\mathbf{a}(\theta)$ are expressed as the direct sum of the corresponding real and imaginary components

$$\mathbf{x} = \begin{bmatrix} \text{Re}\{\mathbf{w}\} \\ \text{Im}\{\mathbf{w}\} \end{bmatrix}, \quad \mathbf{z} = \begin{bmatrix} \text{Re}\{\mathbf{a}\} \\ \text{Im}\{\mathbf{a}\} \end{bmatrix}.$$

The estimated covariance matrix, \mathbf{R}_{yy} , assumed to be positive definite, is written as,

$$\mathbf{R} = \begin{bmatrix} \text{Re}\{\mathbf{R}_{yy}\} & -\text{Im}\{\mathbf{R}_{yy}\} \\ \text{Im}\{\mathbf{R}_{yy}\} & \text{Re}\{\mathbf{R}_{yy}\} \end{bmatrix}.$$

The numerical computations of the algorithm then proceed as follows,

1. Compute $\mathbf{Q} = \mathbf{A}\mathbf{A}^T - \mathbf{c}\mathbf{c}^T$, where \mathbf{A} is the principal matrix square root of \mathbf{P} .
2. Compute the Cholesky factorization of \mathbf{R} , $\mathbf{L}\mathbf{L}^T = \mathbf{R}$.
3. Compute $\mathbf{L}^{-1/2}$.
4. Compute $\tilde{\mathbf{Q}} = \mathbf{L}^{-1/2}\mathbf{Q}(\mathbf{L}^{-1/2})^T$.
5. Compute the eigenvalue decomposition of $\tilde{\mathbf{Q}}$, $\tilde{\mathbf{Q}} = \mathbf{V}\mathbf{T}\mathbf{V}^T$.
6. Change coordinates, as in $\tilde{\mathbf{c}} = \mathbf{V}^T\mathbf{R}^{-1/2}\mathbf{c}$.
7. Find the optimal value, λ^* for the Lagrange multiplier. An approach based on solving a scalar equation is described in [8]. For the results shown in this paper, $\lambda^* = 10$.
8. Compute the optimal weight vector, $\mathbf{x}^* = (\mathbf{R} + \lambda^*\mathbf{Q})^{-1}\mathbf{c}$.

As described in more detail in Section III, the Lorenz beamformer produced the best results of all the beamformers evaluated, and was also the most computationally intensive.

K. Frequency Domain Beamformer

A diagram of the frequency domain beamformer is provided in Fig. 6. In this beamforming configuration, the deramped data is blocked into vectors and transformed into the frequency domain using an FFT. This operation is equivalent to utilizing a DFT filter bank behind each array element. Figure 6 illustrates the polyphase implementation of the analysis and synthesis sections of a DFT filter bank. Further details on DFT filter banks are provided in [9], [10]. Because of the duality between the time domain and the frequency domain for LFM waveforms, the FFT frequency

bins correspond to time cells, or range bins, which can be represented by a tapped delay line. Therefore, this algorithm is analogous to conventional Space-Time Adaptive Processing (STAP) [7].

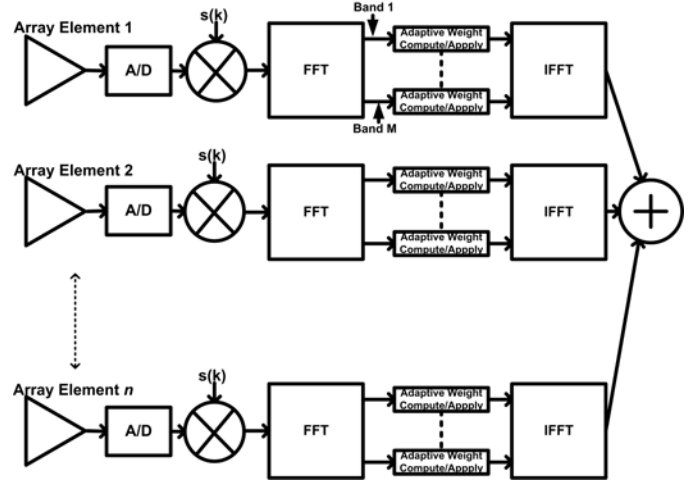


Figure 6 – Frequency Domain Beamformer

III. RESULTS

The performance of each adaptive algorithm under consideration was quantified by locating the two largest peaks across all Doppler frequencies in each range bin. These peaks were manually confirmed to correspond to the direct signal, D , and the target, T . Then the power ratio T/D was computed for the unadapted array output and the adapted array output at identical sample locations. The improvement in T/D ratio, defined as,

$$I = \frac{\left(\frac{T}{D}\right)_{\text{ADAPT}}}{\left(\frac{T}{D}\right)_{\text{UNADAPT}}}$$

was chosen as the metric of increased target detectability and interference cancellation due to adaptive processing. For instance, a ratio I greater than 0 dB indicates that adaptive processing enhanced target power relative to the interfering direct signal power. Statistics were compiled for each adaptive algorithm and compared to determine the algorithm with the best performance. Figure 7 illustrates the array output after the Lorenz beamformer was used to cancel the interference. Now the target track is visible in every range bin.

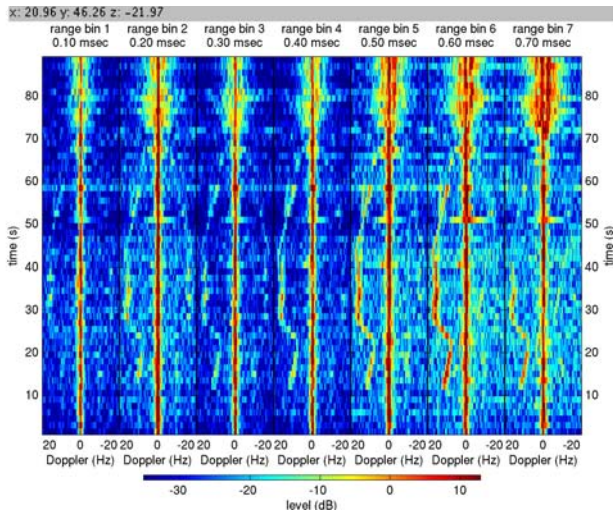


Figure 7 – Output of Lorenz Beamformer

Table 1 summarizes the performance improvement attained using each adaptive algorithm by listing the complementary cumulative probability that the ratio I for a given array output sample is greater than 0 dB. As demonstrated by the data, the Lorenz beamformer yielded the best cancellation performance and all the batch algorithms outperformed the recursive algorithms. A word of caution is appropriate when interpreting the results. First, the difference in performance between algorithms ranked close together, such as the Lorenz beamformer and the frequency domain beamformer is marginal. The difference in performance between algorithms ranked far apart, such as the Lorenz beamformer and the LMS-SP beamformer is much more significant. Second, the performance metric chosen does not capture a lot of second order effects. For example, one could ask, given the fact that there exists some improvement in the T/D ratio at some sample location due to adaptive processing, what is the probability that this improvement is greater than 10 dB, or 20dB? Table 1 does not answer this type of question.

Table 1 – Comparison of Beamformer Algorithms

Algorithm	Probability[$I > 0$ dB]
Lorenz	81%
Frequency Domain	80%
Diagonal Loading	78.7%
Eigenvalue Thresholding	77.7%
Time Domain Segmenting	77.7%
MVDR	77.6%
Covariance Matrix Taper	70.4%
RLS	69.5%
RLS-VL	69.5%
LMS	68.7%
LMS-SP	68.2%

In summary, to understand the overall performance of all 11 algorithms it is quite useful is to visually compare the quality

of the target tracks. Towards this end, Fig. 8 illustrates the adapted output of the LMS-SP algorithm. Here, the target tracks are not as clear or pronounced as at the output of the Lorenz beamformer (Fig. 7), which was determined to yield the best performance of all algorithms.

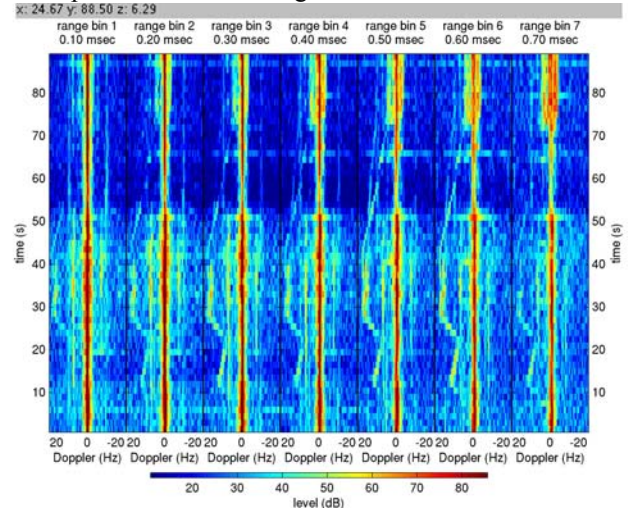


Figure 8 – Output of LMS-SP Beamformer

IV. CONCLUSIONS

Eleven adaptive beamforming algorithms were evaluated for application to mitigating direct signal interference in FBB-HF radar. Of all the algorithms evaluated, the Lorenz beamformer performed best. The Lorenz beamformer is based on explicitly modeling the uncertainties in the array manifold and seems to be most robust in the presence of random errors.

REFERENCES

- [1] G. J. Frazer, "Forward-based Receiver Augmentation for OTHR," *Proc. IEEE Radar Conference*, Boston, MA, April 17-20 2007.
- [2] G. Fabrizio, D. Holdsworth, A. Farina, "Experimental HF Radar Trial of Real-Time STAP," *Proc. International Waveform Diversity and Design Conference*, Pisa, Italy, June 4-8 2007.
- [3] S. Haykin, *Adaptive Filter Theory*, Englewood Cliffs, NJ, Prentice Hall, 1996.
- [4] Z. Tian, K. L. Bell, and H. L. Van Trees, "A Recursive Least Squares Implementation for LCMP Beamforming Under Quadratic Constraint," *IEEE Trans Signal Processing*, vol. 49, pp. 1138-1145, June 2001.
- [5] D. Johnson and D. Dudgeon, *Array Signal Processing: Concepts and Techniques*, ser. Signal Processing, Englewood Cliffs, NJ, Prentice Hall, 1993.
- [6] J. Guerci, "Theory and Application of Covariance Matrix Tapers for Robust Adaptive Beamforming," *IEEE Trans Signal Processing*, vol. 47, pp. 977-985, April 1999.
- [7] J. A. Torres, R. M. Davis, J. D. R. Kramer, R. L. Fante, "Efficient Wideband Jammer Nulling When Using Stretch Processing," *IEEE Trans. Aerospace and Electronic Systems*, vol. 36, pp. 1167-1178, Oct. 2000.
- [8] R. G. Lorenz, "Robust Minimum Variance Beamforming," *IEEE Trans. Signal Processing*, vol. 53, pp. 1684-1696, May 2005.
- [9] P. P. Vaidyanathan, *Multirate Systems and Filter Banks*, Upper Saddle River, NJ, Prentice Hall, 1993.
- [10] F. Lin, K. Gerlach, and M. Picciolo, "Band-Partitioned Sidelobe Canceler for a Wideband Radar," *Proc. IEEE Radar Conference*, Huntsville, AL, May 5-8 2003.